Investigating the Causes and Impacts of Convective Organization in a High Resolution Atmospheric GCM

Bosong Zhang[1], Brian J. Soden[1]

1. Rosenstiel School of Marine and Atmospheric Science

University of Miami, Miami, Florida

Gabriel A. Vecchi[2, 3], Wenchang Yang[2]

2. Department of Geosciences, Princeton University

Princeton, NJ

3. High Meadows Environmental Institute, Princeton University

Princeton, NJ

Corresponding author address: Bosong Zhang, Rosenstiel School of Marine and Atmospheric Science, University of Miami, 4600 Rickenbacker Causeway, Miami, FL 33149, USA. (bosong.zhang@rsmas.miami.edu)

Abstract

A ~ 50 km resolution atmospheric general circulation model (GCM) is used to investigate the impact of radiative interactions on spatial organization of convection, the model's mean state, and extreme precipitation events in the presence of realistic boundary conditions. Mechanism-denial experiments are performed in which synoptic-scale feedbacks between radiation and dynamics are suppressed by overwriting the model-generated atmospheric radiative cooling rates with its monthly-varying climatological values. When synoptic-scale radiative interactions are disabled, the annual mean circulation and precipitation remain almost unchanged, however tropical convection becomes less aggregated, with an increase in cloud fraction and relative humidity in the free troposphere but a decrease in both variables in the boundary layer. Changes in cloud fraction and relative humidity in the boundary layer exhibit more sensitivity to the presence of radiative interactions than variations in the degree of aggregation. The less aggregated state is associated with a decrease in the frequency of extreme precipitation events, coincident with a decrease in the dynamical contribution to the magnitude of extreme precipitation. At regional scales, the spatial contrast in radiative cooling between dry and moist regions diminishes when radiative interactions are suppressed, reducing the upgradient transport of energy, degree of aggregation and frequency of extreme precipitation events. However, the mean width of the tropical rain belt remains almost unaffected when radiative interactions are disabled. These results offer insights into how radiation-circulation

coupling affects the spatial organization of convection, distributions of clouds and humidity, and weather extremes.

Key Points

- Radiative coupling strengthens the degree of aggregation and extreme precipitation.

- Radiative coupling modulates the distribution of clouds and relative humidity.

- Radiative coupling in the boundary layer has comparable impacts on convective organization, clouds and humidity as does radiative coupling in the free troposphere.

Plain Language Summary

Interplays between radiation, clouds and convection are well studied in numerical simulations under idealized boundary conditions (e.g., spatially uniform sea surface temperatures, no wind shear, etc.). However, it remains unclear how they interact with each other in more realistic situations with the presence of sea surface temperature gradients and a large-scale background circulation. In this study we examine the impact of synoptic-scale radiative coupling on convective organization, clouds, and precipitation extremes using a ~50 km resolution atmospheric general circulation model. When synoptic-scale radiative coupling is disabled, we find that the mean circulation and rainfall remain almost unaffected. However, convection becomes less organized without radiative coupling, which is due to the diminished spatial contrast in radiative cooling between dry and moist regions. Also, both daily precipitation and mid-tropospheric updrafts exhibit a reduction in the probability of their extreme values when radiative coupling is disabled. In addition, we find that radiative coupling can modulate the distribution of clouds and relative humidity. These findings highlight the importance of synoptic-scale interactions between radiation and convection even in realistic situations, and motivates the comparison of model simulations and observations.

1 Introduction

The tendency for convection to organize from isolated convective updrafts into spatially coherent clusters has long been recognized in numerical model simulations (Bretherton et al., 2005; Held et al., 1993; Tompkins, 2001). This aggregation of convection occurs even in the presence of uniform boundary conditions (self-organization) and not only impacts the intensity of precipitation events (Bao & Sherwood, 2019), but also modulates the larger-scale thermodynamic

and radiative properties of the tropics (e.g., Bony et al. (2020)). Increased aggregation is associated with increased spatial variance of moisture; dry regions become drier and moist regions become moister (Dai & Soden, 2020). The increased spatial variance of moisture directly impacts both the intensity of precipitating systems and the larger-scale radiative fluxes (Bony et al., 2020; Bony et al., 2016; Bretherton et al., 2005; Wing et al., 2020).

The net effect of more aggregated convection is to dry the tropical free troposphere, particularly in cloud-free regions, resulting in a net loss of longwave radiation to space (Bretherton et al., 2005). This large-scale influence of aggregation has been proposed as a potential thermostat that may regulate the sensitivity of the tropics to radiative forcing (Mauritsen & Stevens, 2015). However, the interaction with radiation involves feedbacks. The amplification and expansion of dry regions is believed to play a key role in triggering aggregation, and radiative feedbacks involving both clouds and water vapor are essential for maintaining the aggregation in idealized models (Wing et al., 2017). Additionally, the relative importance of clear versus cloudy sky radiative processes is not well understood, as is the contributions of shortwave (SW) versus longwave (LW) radiation.

There is a long history of observational studies of convective organization (see Holloway et al. (2017) for a recent review). Most recently, Bony et al. (2020) found that increased aggregation in the tropics is associated with a reduction in high cloud cover, a drier free troposphere in the non-convective environment and increased emission of infrared radiation to space. These features lead to a net radiative cooling of the tropics.

Precipitation extremes are largely controlled by the amount of moisture present in the atmosphere (Allen & Ingram, 2002; Pall et al., 2007; Trenberth, 1999) and also atmospheric convergence (Liu et al., 2020), whereas the global-mean precipitation is constrained by the global-mean radiative cooling. From an energy balance perspective, latent heating into the atmosphere must be balanced by atmospheric radiative cooling given that heat capacity of the atmosphere is negligible (Allen & Ingram, 2002). In model simulations, the change in extreme precipitation in response to increases in greenhouse gases is found to depend on the magnitude of warming (Pendergrass et al., 2015) and the change in convective organization (Muller, 2013; Pendergrass et al., 2016). In observations, the degree of aggregation at regional scales has also been connected with extreme rainfall events (Dai & Soden, 2020).

Climate model projections indicate that the thermodynamic constraint based on the Clausius-Clapeyron relation is a good predictor for extreme precipitation changes in a warmer climate for regions where changes in the circulation are small (Pall et al., 2007). However, this may not be the case for regions with large changes in the atmospheric circulation, such as the tropics (Emori & Brown, 2005; Vecchi & Soden, 2007) or for tropical cyclones (Knutson et al., 2013; Liu et al., 2020). Indeed, several studies suggest that the sensitivity of tropical precipitation extremes is substantially larger than that predicted from

the Clausius-Clapeyron relationship (Allan & Soden, 2008; Norris et al., 2019; O'gorman, 2015; Westra et al., 2013).

Among different factors contributing to radiative cooling of the atmosphere, cloud radiative effects (CRE) have been received considerable attentions. The Clouds On-Off Klimate Intercomparison Experiment (COOKIE) is designed to investigate the role of CRE in the climate system (Stevens et al., 2012). This project compares simulations with clouds that are transparent to radiation ("clouds-off") and those including CRE ("clouds-on"). Using output from the COOKIE project, Fermepin and Bony (2014) showed that low cloud radiative effects increase tropical precipitation and strengthen winds near ocean surface. However, Li et al. (2015) found that CRE can decrease precipitation in the tropics but increase it at middle-to-high latitudes. Recently, Medeiros et al. (2021) reported that extreme precipitation over tropical ocean is strengthened by CRE. While mean precipitation and large-scale circulation can be affected by removing CRE, it is unclear how precipitation, especially extreme precipitation, will respond if radiative-convective interactions are disabled.

In idealized models, studies found that interactive radiation is key to convective aggregation over a limited domain (Muller & Bony, 2015; Muller & Held, 2012; Wing & Emanuel, 2014; Yang, 2018). In simulations of radiative convective equilibrium without rotation, Bao and Sherwood (2019) found that extreme daily precipitation gets stronger when convection is more aggregated with fully interactive radiation. Most research on the coupling of clouds and radiation on smaller time/space scales has focused on the impact of radiative feedbacks on convective organization. These studies typically have been performed using high resolution, radiative equilibrium simulations under very idealized settings. This makes it difficult to ascertain the importance of cloud-circulation feedbacks under more realistic situations (e.g., in the presence of the SST gradients or wind shears that are present in our planet). It also makes it more challenging to evaluate the model simulations with observations.

In this study, we examine the impact of radiative interactions on the spatial organization of convection and extreme precipitation events under realistic boundary conditions. Instead of completely removing the CRE, which dramatically changes the mean circulation and rainfall in a model (e.g., as is done in COOKIE), synoptic-scale radiative interactions are suppressed by prescribing radiative cooling rates using their monthly climatological values. This enables us to examine the behavior of two versions of a model with nearly identical large-scale circulations but with differing degrees of convective organization. Our simulations highlight the role of synoptic-scale radiative coupling in enhancing convective aggregation and extreme precipitation by increasing the horizontal gradient of radiative cooling which provides an upgradient transport of energy from dry to moist regions.

2 Methods

a. Model and experiments

We use the High-Resolution Atmospheric Model (HiRAM; Zhao et al. (2009)) developed at the Geophysical Fluid Dynamics Laboratory (GFDL). All simulations are conducted with prescribed climatological monthly means of sea surface temperature (SST) and sea ice from Hadley Centre Sea Ice and Sea Surface Temperature (HadISST) dataset (Rayner et al., 2003) based on the 20-year period from 1986 to 2005, and are integrated for 50 years with constant atmospheric CO_2, greenhouse gases and aerosol concentrations (at 1990 levels). The first simulation (referred to as the Control run) follows the default model configuration and thus has fully interactive radiation. The second simulation (referred to as the ClimRad run) overwrites the model-generated atmospheric radiative cooling rates with its monthly-varying climatological values computed from the Control run. Specifically, the overwriting process is implemented as follows: (a) monthly atmospheric radiative cooling rates are retrieved from the last 20 years of the Control run; (b) a multiyear average is applied to the 20-year data to get monthly-varying climatological radiative cooling rates; and (c) each time when the radiation code is called in the ClimRad run, the atmospheric radiative cooling rates are overwritten by its monthly-varying climatological values that are temporally interpolated to the current time step. A summary of these simulations is listed in Table 1. These simulations are also used in Zhang et al. (2021).

b. Degree of Convective Aggregation

Different metrics have been used to quantify the degree of aggregation under different circumstances such as the "organization index" that detects organized convective features using satellite observed infrared brightness temperatures (Bony et al., 2020; Tompkins & Semie, 2017), subsidence fraction (Coppin & Bony, 2015), the spatial variance of column relative humidity (Wing & Cronin, 2016) and the spatial variance of column integrated water vapor (Dai & Soden, 2020; Wing et al., 2020). In this study, we characterize the spatial organization of convection using subsidence fraction, which is computed as the fractional area covered by subsidence based on daily vertical pressure velocity at 500 hPa (ω_{500}). We note that using the spatial variance of column integrated water vapor yields similar results.

3 Results

a. Mean circulation and precipitation

Figure 1 shows the zonal mean meridional overturning circulation in the Control and ClimRad runs. Overall the difference between the two simulations is very small, indicating that the mean circulation remains almost unchanged without radiative interactions. Also, we note that suppressing radiative interactions

has little impact on the magnitude of the global-mean precipitation because the overwriting approach applied in the ClimRad run does not change the magnitude of the global-mean radiative cooling of the atmosphere. Overall the atmospheric energy budget remains nearly unaffected in the ClimRad run.

b. Convective aggregation, cloud and relative humidity

Although the mean circulation is essentially the same between the Control and ClimRad runs, suppressing radiative interactions significantly changes features related to synoptic-scale convection. Figure 2 shows probability density functions (PDFs) of daily subsidence fraction in the Control and ClimRad runs computed over the entire tropics (30°S–30°N). Small (large) values of daily subsidence fraction in the ClimRad run are more (less) frequent than those in the Control run, indicating that convection becomes less aggregated when radiative interactions are suppressed. These results are in line with previous numerical simulations with an aquaplanet configuration (Coppin & Bony, 2015) and in convection-resolving models (Muller & Bony, 2015; Muller & Held, 2012; Yang, 2018).

Using satellite observations, Bony et al. (2020) found that the spatial organization of deep convection can modulate high-level clouds and relative humidity in the free troposphere, which further impacts the tropical radiation budget. Based on an ensemble of radiative-convective equilibrium simulations, Wing et al. (2020) showed similar results in which the occurrence of convective self-aggregation reduces high cloud coverage and dries the mid-troposphere. Here, we investigate how clouds and relative humidity respond to suppressed radiative interactions (Figure 3). Negative values are found in the upper troposphere over the tropics for the Control run minus the ClimRad run, indicating that a more aggregated state is associated with fewer high-level clouds. Also, we find that the free troposphere is in general drier in the Control run than that in the ClimRad run (Figure 4). The reduction in high-level clouds and mid-tropospheric relative humidity in the Control run is qualitatively consistent with observations (Bony et al., 2020; Holloway et al., 2017; Stein et al., 2017; Tobin et al., 2013; Tobin et al., 2012) and other model simulations (Bretherton et al., 2005; Wing et al., 2017; Wing & Emanuel, 2014; Wing et al., 2020). This shows that, even when the large-scale circulations are nearly identical, differences in the spatial organization of convection can alter the mean state of the free troposphere.

However, the responses in cloud fraction and relative humidity are not vertically uniform. We find that the Control run has an overall increase in cloud fraction and relative humidity in the boundary layer, which may not be directly linked with the degree of aggregation. Previous results on the relationship between convective aggregation and low cloud fraction are inconclusive. While an increase in low-level clouds with aggregation is found in Tobin et al. (2013) and Stein et al. (2017), Tobin et al. (2012) found the opposite result. Recently, Wing et al. (2020) found that most radiative-convective equilibrium simulations agree on an increase in low-level clouds with convective self-aggregation, although

6

such increase is less robust in magnitude. They proposed that the difference in horizontal grid spacing, rather than the occurrence of self-aggregation itself, may contribute to the increase in low-level clouds. In addition, lower tropospheric stability may also play a role in modulating low-level clouds (Bony et al., 2020). When lower-tropospheric stability increases, more moisture is trapped in the boundary layer, which promotes the formation of low-level clouds (Wood & Bretherton, 2006). However, the impact of lower tropospheric stability on low-level clouds is thought to be independent of the degree of aggregation as noted by Bony et al. (2020). Here we use estimated inversion strength (EIS), defined as $EIS = LTS - \Gamma_m^{850} \left(z_{700} - LCL \right)$, to represent the stability in the boundary layer. LTS stands for lower tropospheric stability and is computed as $LTS = \theta_{700} - \theta_{1000}$ where θ_{700} and θ_{1000} are potential temperatures at 700 hPa and 1000 hPa respectively (Klein & Hartmann, 1993); Γ_m^{850} is

Among different factors contributing to the low cloud fraction, radiative interactions with boundary layer clouds could make a difference. In the boundary layer, the coupling between clouds, radiation, turbulence and entrainment was first documented by Lilly (1968). Strong longwave radiative cooling at the cloud top promotes vertical mixing and drives turbulent eddies, which transports moisture from the sea surface upward and maintains the cloud amount (Bretherton et al., 2004b; Wood, 2012). Additionally, strong radiative cooling at the cloud top increases relative humidity in the boundary layer. Higher relative humidity further promotes the formation of low-level clouds (Brient & Bony, 2012). In the ClimRad run, the coupling between radiation and low-level clouds is disabled, which may explain the reduction in both relative humidity and cloud fraction in the boundary layer.

To explore the sensitivity of clouds and relative humidity to the vertical structure of radiative coupling, we conduct two other simulations: one is referred to as ClimRadFT, in which the overwriting procedure is only applied to the free troposphere, whereas radiation in the boundary layer is fully interactive; the other is referred to as ClimRadBL, in which only radiation in the boundary layer is fixed while that in the free troposphere is interactive (see Table 1 for more details). Compared to the Control run, we find that changes in low-level clouds and lower-tropospheric relative humidity in the ClimRadBL run are similar to those in the ClimRad runs (Figure 3 and Figure 4). In contrast, the differences in tropical low-level clouds and relative humidity in the boundary layer are reduced between the Control and ClimRadFT runs (Figure 3 and Figure 4). However, we note that the ClimRadBL and ClimRadFT runs exhibit similar changes in lower tropospheric stability compared to the Control run (Figure S1). This suggests that it is the direct effects of radiative coupling in the boundary layer that is primarily responsible for the changes in low-level clouds and relative humidity in the ClimRad run, rather than the influence of radiative processes in the free troposphere on lower tropospheric stability.

In addition, the changes in low-level clouds and relative humidity are found to be, at least from a qualitative perspective, independent of variations in the

degree of aggregation. A comparison of the PDFs of daily subsidence fraction from the Control, ClimRad, ClimRadFT and ClimRadBL runs is shown in Figure 5. Compared to the Control run, the other three simulations exhibit an overall reduction in the degree of aggregation although the magnitude of such reduction varies among them. The qualitatively consistent change in the degree of aggregation cannot explain the differing responses in cloud fraction and relative humidity, indicating that variations in the degree of aggregation may not be a leading factor in modulating the distribution of cloud and humidity. Here, the coupling between radiation, cloud and humidity plays a more important role in maintaining the model's mean state.

c. Response in extreme precipitation

Previous idealized modeling studies showed that extreme daily precipitation becomes weaker when convective aggregation is inhibited (Bao & Sherwood, 2019). To examine the response in extreme precipitation to suppressed radiative interactions, we compute the annual maximum daily precipitation (P_e) at each grid point. While the difference in P_e between the Control and ClimRad runs is small at middle-to-high latitudes, a significant reduction in P_e is found across the tropics in the ClimRad run (Figure 6, left), which indicates that suppressing radiative interactions reduces the strength of extreme daily precipitation. At each grid point, P_e can be estimated by a physical scaling diagnostic (O'Gorman & Schneider, 2009; Pfahl et al., 2017; Sugiyama et al., 2010):

$$P_e \sim - \left\{ \omega_e \left. \frac{dq_s}{dp} \right|_{\theta^*} \right\} \#(1)$$

where ω_e is the annual maximum daily vertical pressure velocity, q_s is the saturation specific humidity, p is the pressure and θ^* is the saturation equivalent potential temperature. Here $\{\bullet\}$ means a mass-weighted vertical integral over the troposphere. We show that the scaling approach reproduces the spatial patterns of P_e in both simulations, leading to a consistent reduction in the scaling when radiative interactions are suppressed (Figure 6, right).

Eq. 1 can be used to decompose changes in extreme precipitation into thermodynamic and dynamic contributions. A thermodynamic scaling is implemented by replacing ω_e in Eq. 1 with long-term averaged vertical velocity at each grid point, whereas a dynamic scaling is the difference between the full scaling and the thermodynamic scaling (Pfahl et al., 2017). There is little difference in the thermodynamic contribution between the Control and ClimRad runs (Figure S2, left) because both runs are forced by the same SSTs and CO_2 concentrations. However, the spatial patterns of difference in dynamic contribution (Figure S2, right) largely resemble the spatial patterns of difference in P_e and the scaling, indicating that suppressing radiative interactions primarily reduces the dynamical contribution to extreme precipitation.

To verify the robustness of our results, probability distributions of daily precipitation and updrafts across the tropics (30°S–30°N) are compared between these two simulations. Figure S3 shows the base-10 logarithm of the probability that daily precipitation and mid-tropospheric updrafts ($\omega_{500} < 0$) exceed a particular value in the Control and ClimRad runs. We find that both variables exhibit a reduction in the probability of exceedance toward its extreme values in the ClimRad run, indicating that suppressing radiative interactions reduces the frequency of extreme convective events. We note that suppressing radiative interactions also reduces the temporal variance of daily precipitation (Figure S4).

Having demonstrated the impact of suppressing radiative interactions on convective organization, we next explore the physical mechanisms which underlie these changes. To do that we first divide the tropics into $10° \times 10°$ regional blocks (Figure 7, top). Within each block, the grid point with the local maximum precipitation is identified, which later becomes the new center of that block. The recentered blocks are then composited based on their domain mean precipitation. Here we show composites of precipitation in the Control run for blocks with domain mean precipitation <5, 5–10, 10–15 and >15 mm day^{-1} (Figure 7, bottom). Note that composites of precipitation in the ClimRad run show similar results (not shown). However, the number of blocks per year (referred to as N_b) in each bin is different between the Control and ClimRad runs. Boxplots of N_b normalized by the median value in the Control run are shown in Figure 8 (top). In the >15 mm day^{-1} bin, N_b is reduced in the ClimRad run, which means that blocks with heavy precipitation happen less frequently when radiative interactions are suppressed. Through this block-by-block analysis, we can also compare the degree of aggregation over blocks with similar amplitude of domain mean precipitation. A comparison of PDFs of daily subsidence fraction between the Control and ClimRad runs are shown in Figure 8 (bottom). Higher probabilities of large subsidence fraction are found in the Control run, indicating that suppressing radiative interactions leads to an overall reduction in aggregation across convective systems of different intensities, which is consistent with the results shown in Figure 2.

In idealized models, it is found that the upgradient transport of moist static energy (Neelin & Held, 1987) plays an important role in convective aggregation (Bretherton et al., 2005; Muller & Bony, 2015; Muller & Held, 2012). Here, radiative cooling and circulation are composited over bins as shown in Figure 8. Following Bretherton et al. (2005), we use column relative humidity (CRH), defined as the ratio of water vapor path to the saturation water vapor path of the atmospheric column (Bretherton et al., 2004a; Raymond, 2000), to represent the degree of dryness at each grid point within a block. Next, all grid points in a block are sorted from lowest to highest CRH and the circulation is represented by an effective streamfunction Ψ, which is computed as a horizontal integral over vertical velocity starting with the driest grid point. The streamfunction Ψ at a certain grid point can be interpreted as an accumulation of vertical mass flux over grid points that are drier than the target grid point. Primarily,

9

the streamfunction is thought to capture the exchange of moist static energy between dry and moist regions (Bretherton et al., 2005).

Figure 9 shows the streamfunction Ψ and radiative cooling rates in the Control and ClimRad runs. In the Control run, when the domain mean precipitation is small, the circulation is weak and there is little contrast in radiative cooling between dry and moist regions, especially in the lower troposphere. As the domain mean precipitation increases, the circulation gets stronger, with its low-level component below ~850 hPa moving air from dry to moist regions. Although the magnitude of radiative cooling in dry regions does not change much, the radiative cooling reduces significantly in moist regions as domain mean precipitation increases, which is equivalent to adding anomalous radiative heating there. As a result, the horizontal gradient of radiative cooling is enhanced, which promotes the low-level circulation and thus the upgradient transport of energy. In comparison, the enhanced horizontal gradient of radiative cooling shown in the Control run is missing in the ClimRad run, indicating that suppressing radiative interactions inhibits the horizontal gradient of radiative cooling from increasing, which explains why the degree of aggregation and extreme precipitation events are reduced in the ClimRad run.

d. Meridional width of the tropical rain belt

Recent studies measure the width of tropical ascending regions by the fraction of vertical pressure velocity at 500 hPa less than zero in the tropics (Su et al., 2020; Su et al., 2019). Given the same domain, greater ascending fraction corresponds to smaller subsidence fraction. While in section 3b we show that daily subsidence fraction in the tropics is reduced without radiative interactions. On longer time scales, the mean vertical pressure velocity at 500 hPa exhibits little difference between the Control and ClimRad runs (not shown). However, this definition may not be an appropriate measure of the meridional width of zonal mean Hadley circulation or the width of the intertropical convergence zone (ITCZ), as noted by Su et al. (2020). Therefore, other metrics are required to quantify the width of the tropical rain belt. Based on observations, Popp and Bony (2019) reported a strong link between zonal convective clustering (CC) and the tropical rain belt: when convection becomes more clustered in the zonal direction, the meridional width of tropical rain belt increases and exhibits a double-peak structure. However, it remains unclear how CC is related to the width of ITCZ in climate models (Popp et al., 2020b). In section 3b, we show that suppressing radiative interactions reduces the degree of aggregation across the tropics. Thus, convection should become less clustered in the zonal direction as well without radiative interactions. Here, two metrics are used to characterize zonal CC: i) the precipitation-inferred CC index, which is defined as monthly mean of the meridionally averaged daily zonal standard deviation of precipitation from 6°S to 6°N normalized by the daily mean precipitation over the same region (Popp & Bony, 2019); and ii) the dynamically inferred CC index, which is defined as the monthly average of the daily zonal fraction of positive

values of the meridional-mean vertical pressure velocity at 500 hPa between 6°S to 6°N (Popp et al., 2020a). Also, we only consider months during which the tropical precipitation distribution is symmetric about the equator with the tropical precipitation asymmetry index (Hwang & Frierson, 2013; Popp & Bony, 2019) less than 0.4. Another two metrics are used to quantify the ITCZ width: i) the precipitation-inferred ITCZ width, which is defined as the area mean of precipitation from 15°S to 15°N divided by the area mean of precipitation from 6°S to 6°N (Popp & Bony, 2019); and ii) the dynamically inferred ITCZ width, which is defined by the contiguous width in degrees latitude of zonal mean ascent region at 500 hPa around the absolute maximum of zonal mean precipitation (Byrne & Schneider, 2016; Popp & Bony, 2019).

Scatter plots of zonal CC and the ITCZ width in the Control and ClimRad runs are shown in Figure 10. Positive temporal correlations are found between zonal CC and the ITCZ width using either precipitation or dynamically inferred metrics in both simulations, which is consistent with observations (Popp & Bony, 2019). We note that the mean ITCZ width exhibits little difference between the Control and ClimRad runs, which is supported by Figure S5 and Figure S6 based on precipitation minus evaporation. These results indicate that suppressing radiative interactions has little impact on the mean ITCZ width. In comparison, the mean value of zonal CC is reduced in the ClimRad run, which comes as no surprise since the degree of aggregation is also reduced without radiative interactions as illustrated in section 3b. Based on model simulations participating in CMIP5 (Taylor et al., 2012), Popp et al. (2020b) showed that biases in CC cannot explain biases in the ITCZ width and no dominant mechanism could explain the link between the temporal variability of CC and that of the ITCZ width. However, they found a tendency for models with higher spatial resolution to exhibit stronger links between zonal CC and the dynamically inferred ITCZ width. In this study, suppressing radiative interactions has a robust impact on zonal CC but little impact on the mean ITCZ width. One possibility is that while the degree of aggregation/clustering is more sensitive to synoptic-scale radiation-circulation coupling (i.e. the spatial contrast in radiative cooling), the ITCZ width is more dependent on the long-term averaged large-scale circulation in this GCM.

4 Summary and Discussion

This study examines the impact of radiative interactions on the spatial organization of convection, the distribution of clouds and relative humidity, and extreme daily precipitation events. We show that suppressing radiative interactions does not alter the mean circulation much but reduces the degree of convective aggregation. The reduction in the degree of aggregation is associated with an increase in high cloud coverage and relative humidity in the free troposphere and a decrease in the boundary layer. These differing responses of cloud and humidity are found to be sensitive to radiative interactions and, to

some extent, independent of variations in the degree of aggregation.

Additionally, a less aggerated state due to suppressed radiative interactions is associated with a decrease in the frequency of extreme precipitation events due to a reduction in the dynamic contribution, i.e., a weakening of the strongest updrafts. At regional scales, suppressing radiative interactions diminishes the horizontal gradient of radiative cooling from dry to moist regions, weakening the upgradient transport of energy and reducing the degree of aggregation. However, the mean ITCZ width shows little difference with and without radiative interactions.

While our results show that the impact of radiative interactions on the degree of aggregation and extreme precipitation is not overwhelmed by the presence of realistic SST gradients, it is worth mentioning that the model response to suppressed radiative interactions shows considerable spatial variability. Overall, stronger signals are found in the tropics than those at mid to high latitudes. Signals over sea surfaces are also more robust than those over land ones. These spatially heterogeneous responses indicate that local environment may play a role in determining the extent to which radiative interactions impact extreme weather extremes and convective aggregation. In addition, our simulations are performed with prescribed SSTs, which essentially excludes the possible impact of changes in the degree of aggregation on SSTs. It remains unclear whether and how changes in the degree of aggregation affect SSTs, and if yes, how changes in SSTs would feedback onto interactions between radiation and convection. Future studies may explore these issues using fully coupled GCMs.

Acknowledgement

References

Allan, R. P., & Soden, B. J. (2008). Atmospheric warming and the amplification of precipitation extremes. *Science, 321*(5895), 1481-1484. Allen, M. R., & Ingram, W. J. (2002). Constraints on future changes in climate and the hydrologic cycle. *Nature, 419*(6903), 228-232. Bao, J., & Sherwood, S. C. (2019). The Role of Convective Self-Aggregation in Extreme Instantaneous Versus Daily Precipitation. *Journal of Advances in Modeling Earth Systems, 11*(1), 19-33. Bony, S., Semie, A., Kramer, R., Soden, B., Tompkins, A., & Emanuel, K. (2020). Observed modulation of the tropical radiation budget by

deep convective organization and lower-tropospheric stability. *AGU Advances, 1*(3), e2019AV000155. Bony, S., Stevens, B., Coppin, D., Becker, T., Reed, K. A., Voigt, A., & Medeiros, B. (2016). Thermodynamic control of anvil cloud amount. *Proceedings of the National Academy of Sciences, 113*(32), 8927-8932. Bretherton, C. S., Blossey, P. N., & Khairoutdinov, M. (2005). An energy-balance analysis of deep convective self-aggregation above uniform SST. *Journal of the Atmospheric Sciences, 62*(12), 4273-4292. Bretherton, C. S., Peters, M. E., & Back, L. E. (2004a). Relationships between water vapor path and precipitation over the tropical oceans. *Journal of Climate, 17*(7), 1517-1528. Bretherton, C. S., Uttal, T., Fairall, C. W., Yuter, S. E., Weller, R. A., Baumgardner, D., et al. (2004b). The EPIC 2001 stratocumulus study. *Bulletin of the American Meteorological Society, 85*(7), 967-978. Brient, F., & Bony, S. (2012). How may low-cloud radiative properties simulated in the current climate influence low-cloud feedbacks under global warming? *Geophysical Research Letters, 39*(20). Byrne, M. P., & Schneider, T. (2016). Energetic constraints on the width of the intertropical convergence zone. *Journal of Climate, 29*(13), 4709-4721. Coppin, D., & Bony, S. (2015). Physical mechanisms controlling the initiation of convective self-aggregation in a general circulation model. *Journal of Advances in Modeling Earth Systems, 7*(4), 2060-2078. Dai, N., & Soden, B. J. (2020). Convective aggregation and the amplification of tropical precipitation extremes. *AGU Advances, 1*(4), e2020AV000201. Emori, S., & Brown, S. (2005). Dynamic and thermodynamic changes in mean and extreme precipitation under changed climate. *Geophysical Research Letters, 32*(17). Fermepin, S., & Bony, S. (2014). Influence of low-cloud radiative effects on tropical circulation and precipitation. *Journal of Advances in Modeling Earth Systems, 6*(3), 513-526. Held, I. M., Hemler, R. S., & Ramaswamy, V. (1993). Radiative-convective equilibrium with explicit two-dimensional moist convection. *Journal of Atmospheric Sciences, 50*(23), 3909-3927. Holloway, C. E., Wing, A. A., Bony, S., Muller, C., Masunaga, H., L'Ecuyer, T. S., et al. (2017). Observing convective aggregation. *Surveys in Geophysics, 38*(6), 1199-1236. Hwang, Y.-T., & Frierson, D. M. (2013). Link between the double-Intertropical Convergence Zone problem and cloud biases over the Southern Ocean. *Proceedings of the National Academy of Sciences, 110*(13), 4935-4940. Klein, S. A., & Hartmann, D. L. (1993). The seasonal cycle of low stratiform clouds. *Journal of Climate, 6*(8), 1587-1606. Knutson, T. R., Sirutis, J. J., Vecchi, G. A., Garner, S., Zhao, M., Kim, H.-S., et al. (2013). Dynamical downscaling projections of 21st century Atlantic hurricane activity: CMIP3 and CMIP5 model-based scenario. *J. Climate, 26*, 6591-6617. Li, Y., Thompson, D. W., & Bony, S. (2015). The influence of atmospheric cloud radiative effects on the large-scale atmospheric circulation. *Journal of Climate, 28*(18), 7263-7278. Lilly, D. K. (1968). Models of cloud-topped mixed layers under a strong inversion. *Quarterly Journal of the Royal Meteorological Society, 94*(401), 292-309. Liu, M., Yang, L., Smith, J., & Vecchi, G. (2020). Response of extreme rainfall for landfalling tropical cyclones undergoing extratropical transition to projected climate change: Hurricane Irene (2011). *Earth's Future, 8*(3), e2019EF001360. Mauritsen, T., & Stevens, B. (2015). Missing iris effect as a possible cause of muted hydrological

change and high climate sensitivity in models. *Nature Geoscience, 8*(5), 346. Medeiros, B., Clement, A. C., Benedict, J. J., & Zhang, B. (2021). Investigating the impact of cloud-radiative feedbacks on tropical precipitation extremes. *npj Climate and Atmospheric Science, 4*(1), 1-10. Muller, C. (2013). Impact of convective organization on the response of tropical precipitation extremes to warming. *Journal of Climate, 26*(14), 5028-5043. Muller, C., & Bony, S. (2015). What favors convective aggregation and why? *Geophysical Research Letters, 42*(13), 5626-5634. Muller, C. J., & Held, I. M. (2012). Detailed investigation of the self-aggregation of convection in cloud-resolving simulations. *Journal of the Atmospheric Sciences, 69*(8), 2551-2565. Neelin, J. D., & Held, I. M. (1987). Modeling tropical convergence based on the moist static energy budget. *Monthly Weather Review, 115*(1), 3-12. Norris, J., Chen, G., & Neelin, J. D. (2019). Thermodynamic versus dynamic controls on extreme precipitation in a warming climate from the Community Earth System Model Large Ensemble. *Journal of Climate, 32*(4), 1025-1045. O'Gorman, P. A., & Schneider, T. (2009). The physical basis for increases in precipitation extremes in simulations of 21st-century climate change. *Proceedings of the National Academy of Sciences, 106*(35), 14773-14777. O'Gorman, P. A. (2015). Precipitation extremes under climate change. *Current Climate Change Reports, 1*(2), 49-59. Pall, P., Allen, M., & Stone, D. A. (2007). Testing the Clausius–Clapeyron constraint on changes in extreme precipitation under CO 2 warming. *Climate Dynamics, 28*(4), 351-363. Pendergrass, A. G., Lehner, F., Sanderson, B. M., & Xu, Y. (2015). Does extreme precipitation intensity depend on the emissions scenario? *Geophysical Research Letters, 42*(20), 8767-8774. Pendergrass, A. G., Reed, K. A., & Medeiros, B. (2016). The link between extreme precipitation and convective organization in a warming climate: Global radiative-convective equilibrium simulations. *Geophysical Research Letters, 43*(21), 11,445-411,452. Pfahl, S., O'Gorman, P. A., & Fischer, E. M. (2017). Understanding the regional pattern of projected future changes in extreme precipitation. *Nature Climate Change, 7*(6), 423-427. Popp, M., & Bony, S. (2019). Stronger zonal convective clustering associated with a wider tropical rain belt. *Nature communications, 10*(1), 1-12. Popp, M., Lutsko, N. J., & Bony, S. (2020a). The relationship between convective clustering and mean tropical climate in aquaplanet simulations. *Journal of Advances in Modeling Earth Systems, 12*(8), e2020MS002070. Popp, M., Lutsko, N. J., & Bony, S. (2020b). Weaker links between zonal convective clustering and ITCZ width in climate models than in observations. *Geophysical Research Letters, 47*(22), e2020GL090479. Raymond, D. J. (2000). Thermodynamic control of tropical rainfall. *Quarterly Journal of the Royal Meteorological Society, 126*(564), 889-898. Rayner, N., Parker, D. E., Horton, E., Folland, C. K., Alexander, L. V., Rowell, D., et al. (2003). Global analyses of sea surface temperature, sea ice, and night marine air temperature since the late nineteenth century. *Journal of Geophysical Research: Atmospheres, 108*(D14). Stein, T. H., Holloway, C. E., Tobin, I., & Bony, S. (2017). Observed relationships between cloud vertical structure and convective aggregation over tropical ocean. *Journal of Climate, 30*(6), 2187-2207. Stevens, B., Bony, S., & Webb, M. (2012). Clouds on-off klimate intercomparison experiment (COOKIE). Su, H., Wu, L.,

Zhai, C., Jiang, J. H., Neelin, J. D., & Yung, Y. L. (2020). Observed tightening of tropical ascent in recent decades and linkage to regional precipitation changes. *Geophysical Research Letters, 47*(3), e2019GL085809. Su, H., Zhai, C., Jiang, J. H., Wu, L., Neelin, J. D., & Yung, Y. L. (2019). A dichotomy between model responses of tropical ascent and descent to surface warming. *npj Climate and Atmospheric Science, 2*(1), 1-8. Sugiyama, M., Shiogama, H., & Emori, S. (2010). Precipitation extreme changes exceeding moisture content increases in MIROC and IPCC climate models. *Proceedings of the National Academy of Sciences, 107*(2), 571-575. Taylor, K. E., Stouffer, R. J., & Meehl, G. A. (2012). An overview of CMIP5 and the experiment design. *Bulletin of the American Meteorological Society, 93*(4), 485-498. Tobin, I., Bony, S., Holloway, C. E., Grandpeix, J. Y., Seze, G., Coppin, D., et al. (2013). Does convective aggregation need to be represented in cumulus parameterizations? *Journal of Advances in Modeling Earth Systems, 5*(4), 692-703. Tobin, I., Bony, S., & Roca, R. (2012). Observational evidence for relationships between the degree of aggregation of deep convection, water vapor, surface fluxes, and radiation. *Journal of Climate, 25*(20), 6885-6904. Tompkins, A. M. (2001). Organization of tropical convection in low vertical wind shears: The role of cold pools. *Journal of the Atmospheric Sciences, 58*(13), 1650-1672. Tompkins, A. M., & Semie, A. G. (2017). Organization of tropical convection in low vertical wind shears: Role of updraft entrainment. *Journal of Advances in Modeling Earth Systems, 9*(2), 1046-1068. Trenberth, K. E. (1999). Conceptual framework for changes of extremes of the hydrological cycle with climate change. In *Weather and climate extremes* (pp. 327-339): Springer.Vecchi, G. A., & Soden, B. J. (2007). Global warming and the weakening of the tropical circulation. *Journal of Climate, 20*(17), 4316-4340. Westra, S., Alexander, L. V., & Zwiers, F. W. (2013). Global increasing trends in annual maximum daily precipitation. *Journal of Climate, 26*(11), 3904-3918. Wing, A. A., & Cronin, T. W. (2016). Self-aggregation of convection in long channel geometry. *Quarterly Journal of the Royal Meteorological Society, 142*(694), 1-15. Wing, A. A., Emanuel, K., Holloway, C. E., & Muller, C. (2017). Convective self-aggregation in numerical simulations: A review. In *Shallow Clouds, Water Vapor, Circulation, and Climate Sensitivity* (pp. 1-25): Springer.Wing, A. A., & Emanuel, K. A. (2014). Physical mechanisms controlling self-aggregation of convection in idealized numerical modeling simulations. *Journal of Advances in Modeling Earth Systems, 6*(1), 59-74. Wing, A. A., Stauffer, C. L., Becker, T., Reed, K. A., Ahn, M. S., Arnold, N. P., et al. (2020). Clouds and Convective Self-Aggregation in a Multi-Model Ensemble of Radiative-Convective Equilibrium Simulations. *Journal of Advances in Modeling Earth Systems*, e2020MS002138. Wood, R. (2012). Stratocumulus clouds. *Monthly Weather Review, 140*(8), 2373-2423. Wood, R., & Bretherton, C. S. (2006). On the relationship between stratiform low cloud cover and lower-tropospheric stability. *Journal of Climate, 19*(24), 6425-6432. Yang, D. (2018). Boundary Layer Diabatic Processes, the Virtual Effect, and Convective Self-Aggregation. *Journal of Advances in Modeling Earth Systems, 10*(9), 2163-2176. Zhang, B., Soden, B. J., Vecchi, G. A., & Yang, W. (2021). The role of radiative interactions in tropical cyclone development under realistic

boundary conditions. *Journal of Climate, 34*(6), 2079-2091. Zhao, M., Held, I. M., Lin, S.-J., & Vecchi, G. A. (2009). Simulations of global hurricane climatology, interannual variability, and response to global warming using a 50-km resolution GCM. *Journal of Climate, 22*(24), 6653-6678.

Tables

Table 1 A list of the simulations conducted in this study.

Experiment name	SST forcing	CO$_2$ forcing	Radiation
Control	1986-2005 Average	Fixed	Fully Interactive
ClimRad	1986-2005 Average	Fixed	Prescribed Climatology
ClimRadFT	1986-2005 Average	Fixed	Prescribed Climatology in the Free Troposphere (fron
ClimRadBL	1986-2005 Average	Fixed	Prescribed Climatology in the Boundary Layer (belov
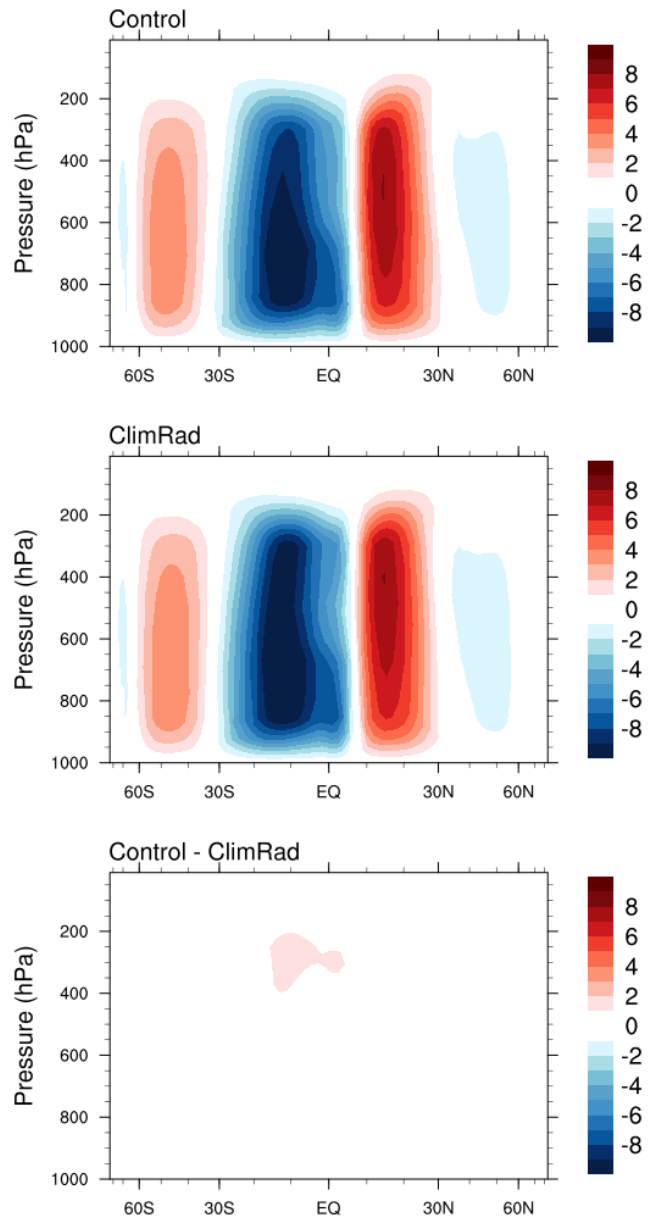
Figures

Figure 1 Annual mean, zonal mean meridional circulation by stream function (unit: $\times 10^{10}$ kg s^{-1}) in the Control run (top), ClimRad run (middle) and their difference (bottom).
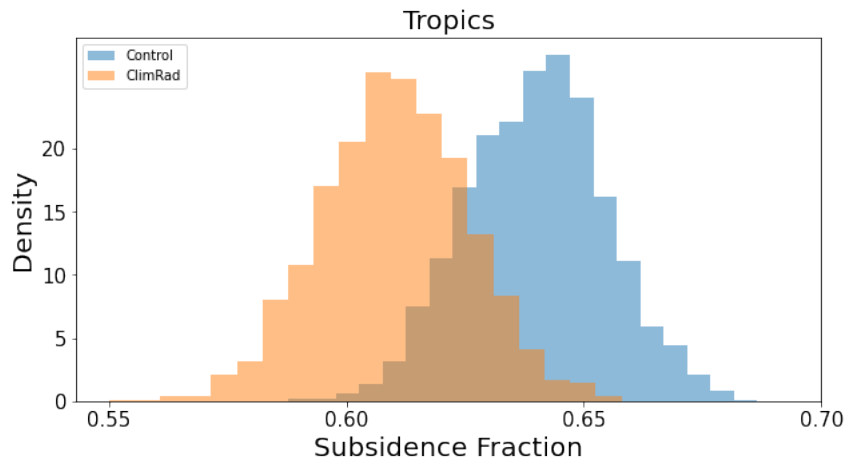
Figure 2 PDFs of the subsidence fraction in the Control and ClimRad runs over the entire tropics. The two PDFs are significantly different based on the Kolmogorov-Smirnov two-sample test with *p value* less than 0.01.
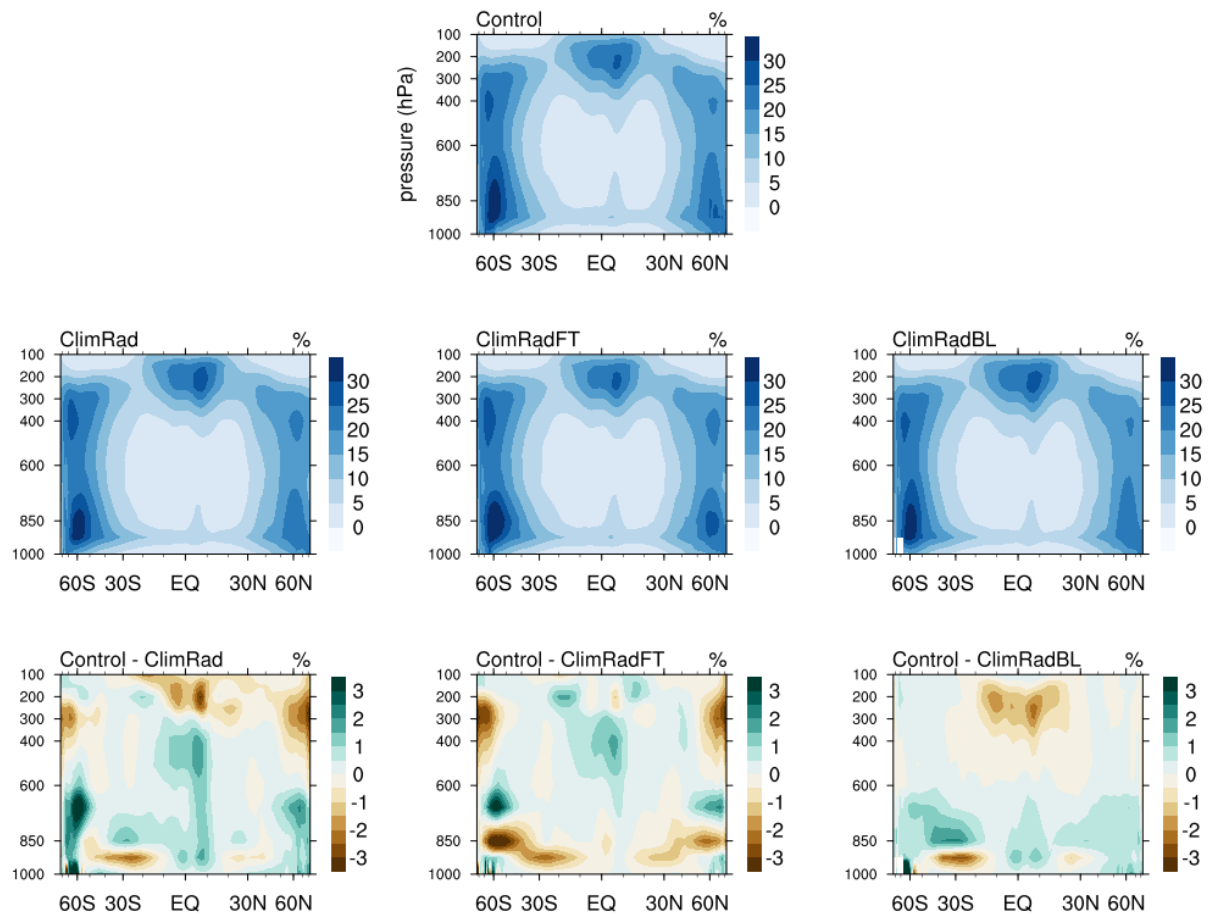
Figure 3 Vertical distribution of zonal mean cloud fraction (unit: %) in the Control run (top row), the ClimRad, ClimRadFT and ClimRadBL runs (middle row, from left to right) and their difference (bottom row). The y-axis (pressure) is of logarithmic scale.
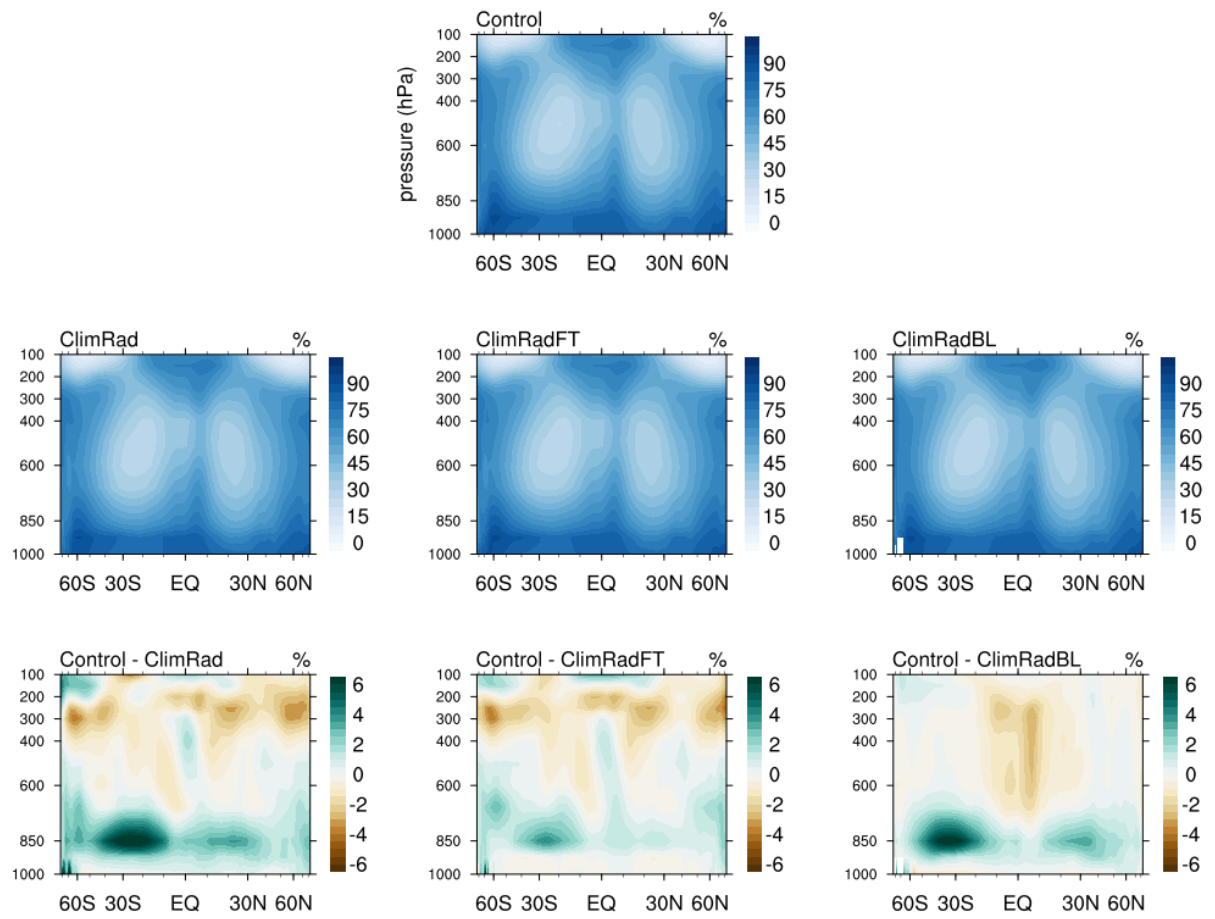
Figure 4 Same as Figure 3 but for vertical distribution of zonal mean relative humidity (unit: %).
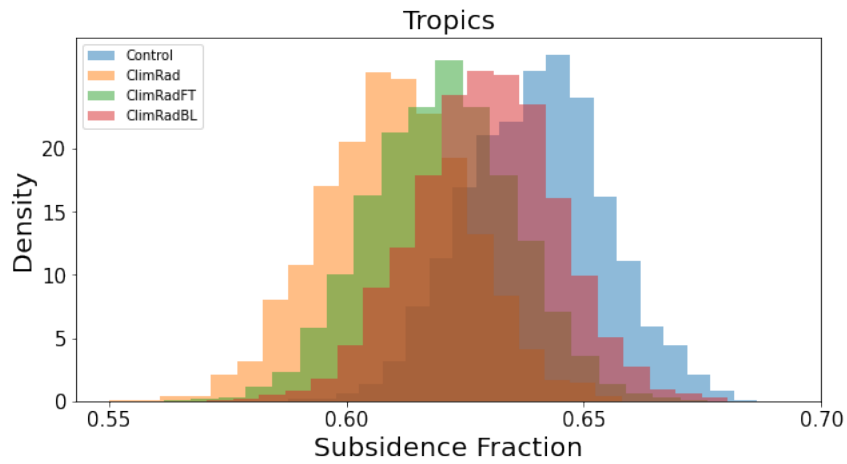
Figure 5 A comparison of PDFs of the subsidence fraction in the Control, ClimRad, ClimRadFT and ClimRadBL runs over the entire tropics.
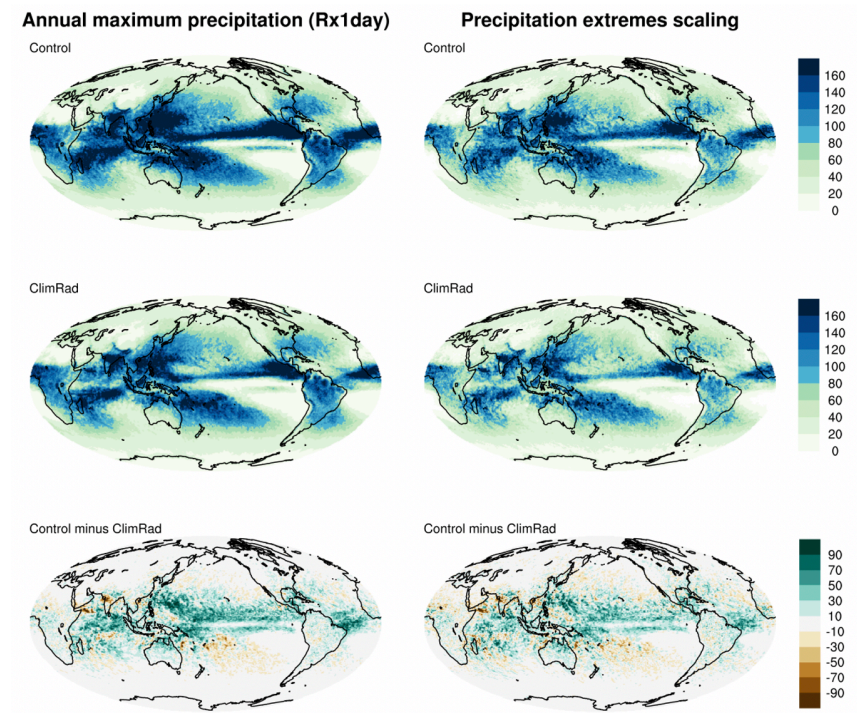
Figure 6 Maps of annual maximum precipitation (left; units: mm day^{-1}) and precipitation extremes scaling (right; units: mm day^{-1}) in the Control run (top), ClimRad run (middle) and their difference (bottom).

21
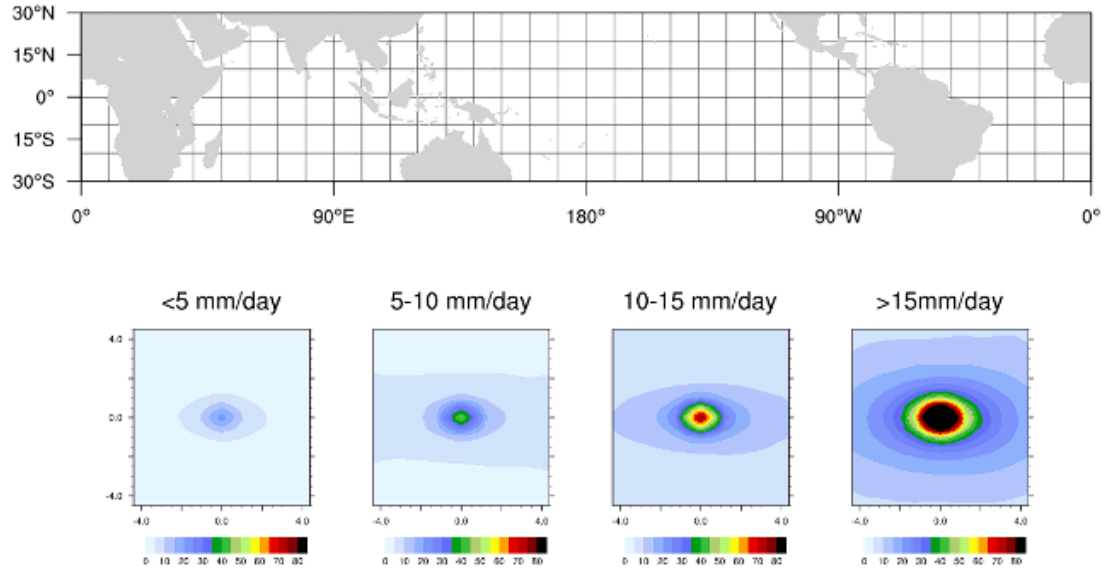
Figure 7 The top row shows $10° \times 10°$ blocks across the tropics while the bottom row shows composites of precipitation in the Control run for different domain mean precipitation bins: <5, 5–10, 10–15 and >15 mm day^{-1} (from left to right).
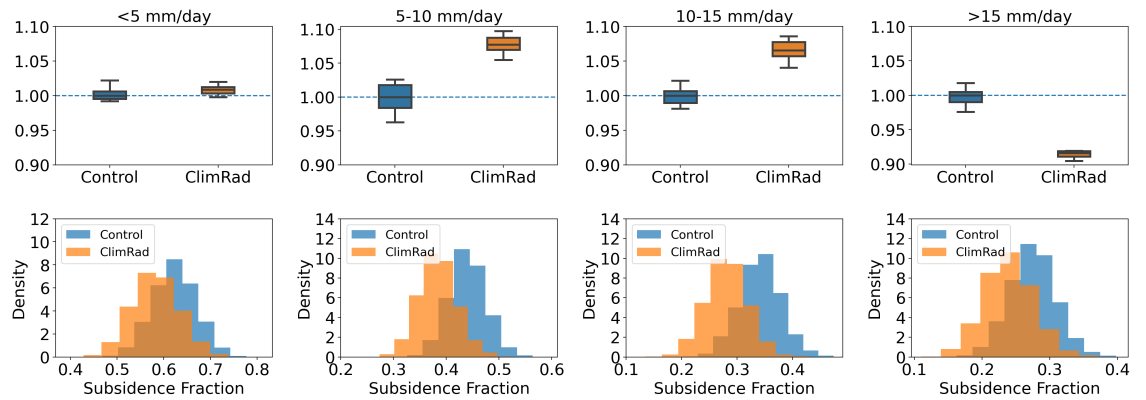
Figure 8 The top row shows boxplots of normalized N_b in the Control run (red) and the ClimRad run (blue), while the bottom row shows PDFs of subsidence fraction.
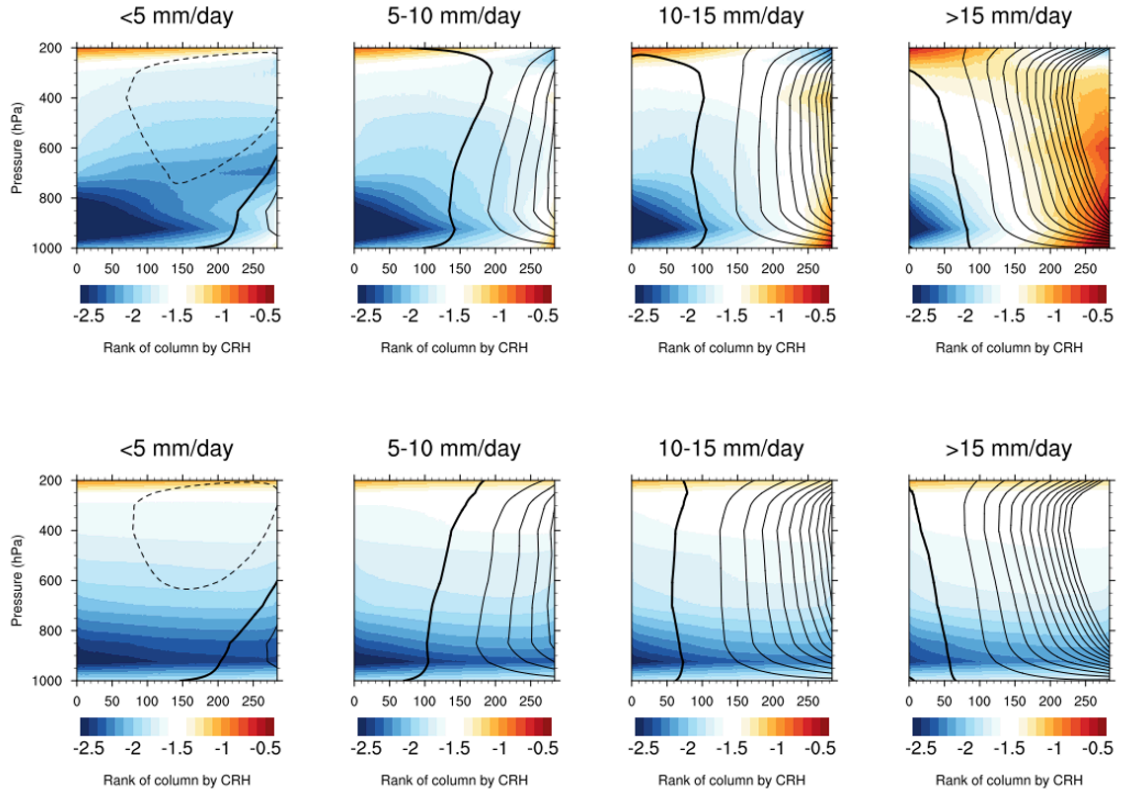
Figure 9 Composites of CRH-sorted streamfunction (contours; the thicker solid line shows zero values) and radiative cooling rates (colors; K day^{-1}) for the Control run (top) and the ClimRad run (bottom) for different domain average precipitation bins.
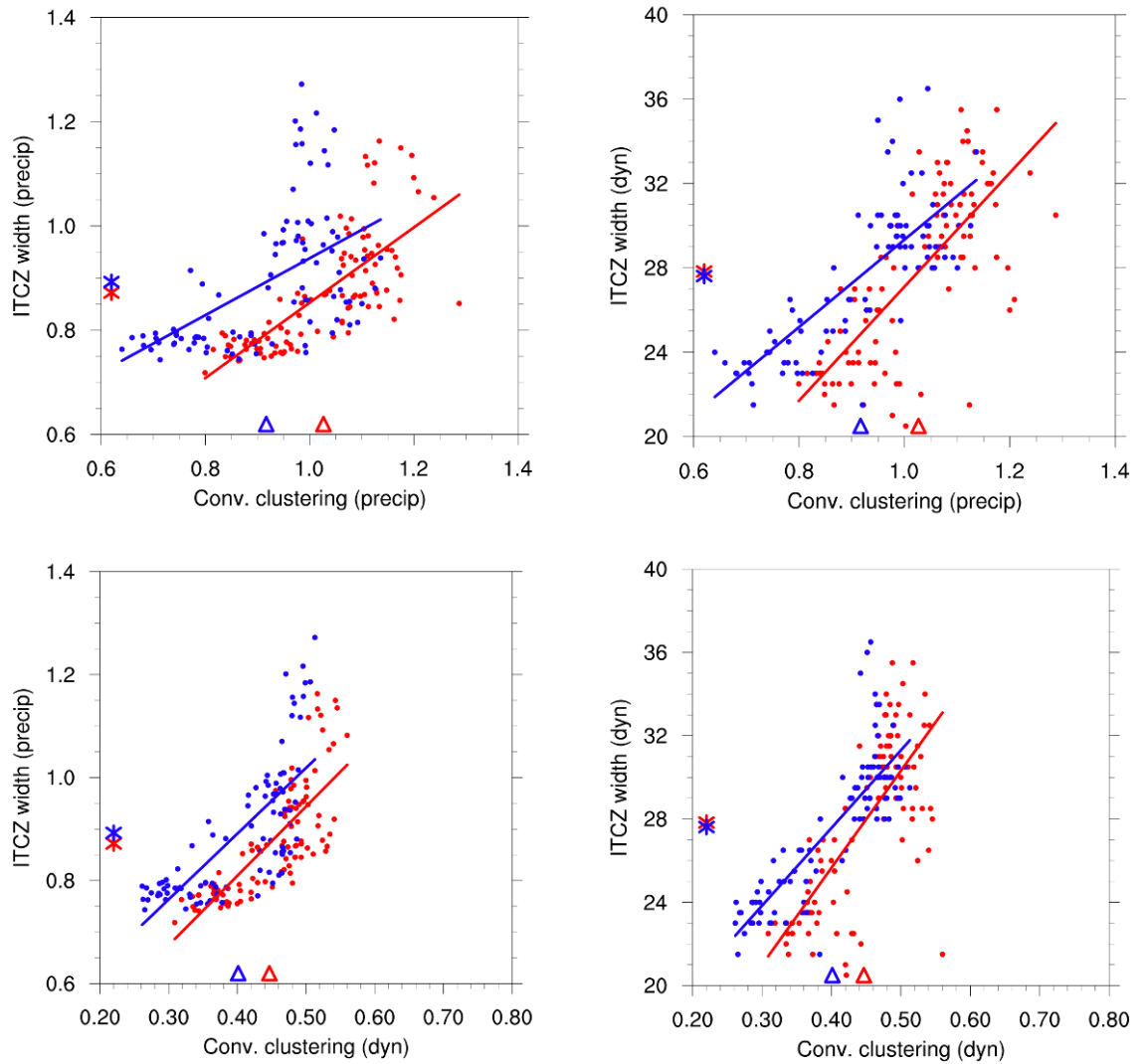
Figure 10 Scatter plots of two metrics for the zonal CC (x-axis) and two metrics for the ITCZ width (y-axis) in the Control run (red) and the ClimRad run (blue). Mean values of the zonal CC (the ITCZ width) are marked with triangles (asterisks). Results are computed over months during which the tropical precipitation distribution is symmetric about the equator.

Supplementary
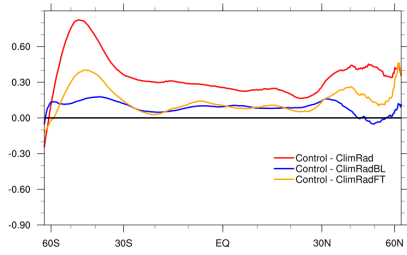
Figure S1 Zonal mean difference in EIS for Control – ClimRad (the red line),
Control – ClimRadBL (the blue line), and Control – ClimRadFT (the orange
line).
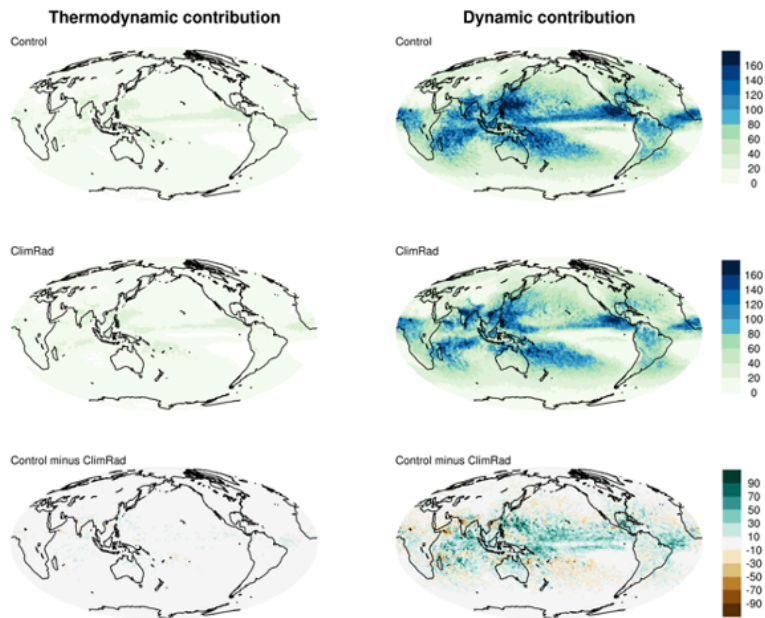
Figure S2 Same as Figure 6 but for the thermodynamic contribution (left; units: mm day^{-1}) and the dynamic contribution (right; units: mm day^{-1}). See texts in section 3c for more details.
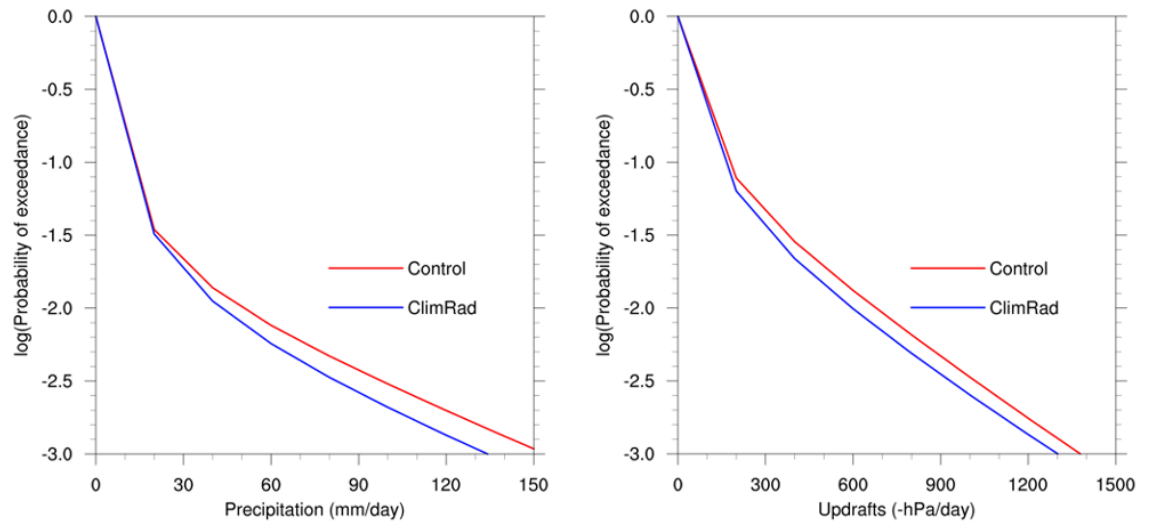

Figure S3 Logarithmic probabilities of exceedance for daily precipitation (left) and daily updrafts at 500 hPa (right) over grid points within the tropics (30°S–30°N) for the Control run (red lines) and the ClimRad run (blue lines).
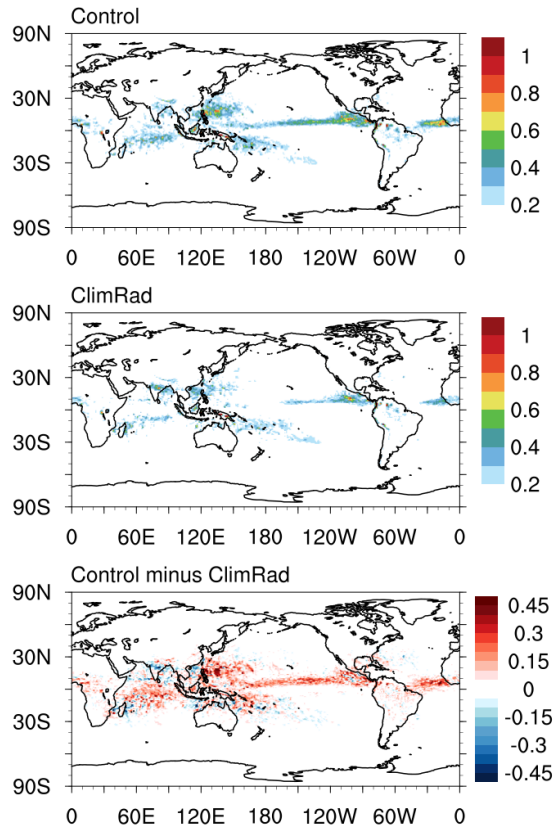
Figure S4 Maps of temporal variance of daily precipitation (units: $\times 10^3$ mm^2 day^{-2}) in the Control run (top), ClimRad run (middle) and their difference (bottom).
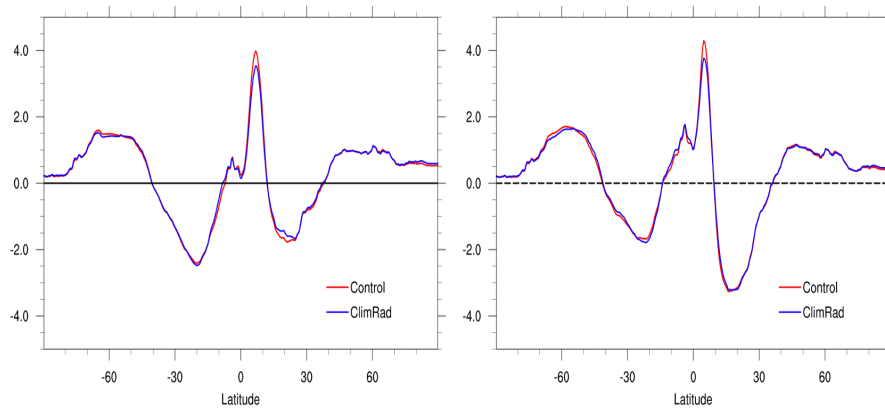
Figure S5 Zonal mean P minus E (units: mm day^{-1}) averaged over all months (left) and over months during which the tropical precipitation distribution is symmetric about the equator (right).
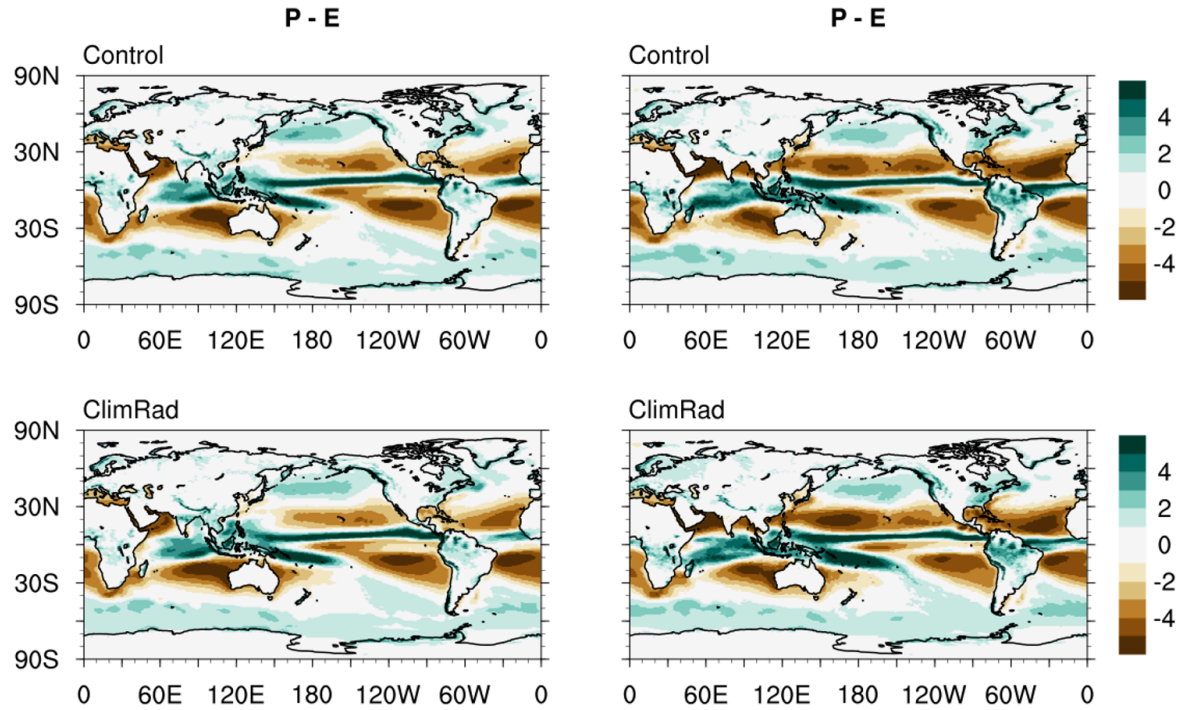

Figure S6 Maps of P minus E (units: mm day^{-1}) for the Control run (top) and the ClimRad run (bottom) averaged over all months (left) and over months during which the tropical precipitation distribution is symmetric about the equator (right).